

Microstructures and Mechanical Properties of Weld Metal and Heat-Affected Zone of Electron Beam-Welded Joints of HG785D Steel

Qiang Zhang, Jianmin Han, Caiwang Tan, Zhiyong Yang, and Junqiang Wang

(Submitted April 29, 2016; in revised form September 14, 2016; published online November 3, 2016)

Vacuum electron beam welding (EBW) process was employed to butt weld 10-mm-thick HG785D high-strength steels. The penetration into the steel was adjusted by beam current. Microstructures at weld metal and heat-affected zone (HAZ) regions were comparatively observed. Mechanical properties of the EBWed joints including Vickers hardness, tensile and Charpy impact tests were evaluated. The results indicated that microstructures at the weld metal consisted of coarse lath martensite and a small amount of acicular martensite, while that in the HAZ was tempered sorbite and martensite. The grain size in the weld metal was found to be larger than that in the HAZ, and its proportion in weld metal was higher. The hardness in the weld metal was higher than the HAZ and base metal. The tensile strength and impact toughness in the HAZ was higher than that in the weld metal. All the behaviors were related to microstructure evolution caused by higher cooling rates and state of base metal. The fracture surfaces of tensile and impact tests on the optimized joint were characterized by uniform and ductile dimples. The results differed significantly from that obtained using arc welding process.

Keywords EBSD, electron beam welding, high-strength steel, microstructure

1. Introduction

Because of its low coefficient of thermal expansion, high yield strength and tensile strength, HG785D steel has been extensively used in the heavy steel structure components, such as shipbuilding, pressure vessel, crane frame and high-speed train. The weldability of the steel was investigated because of its high carbon content and large amount of alloying element. The tendency of welding crack and coarse martensite would easily increase especially for thick plates if the inappropriate welding process was employed.

The conventional welding methods for HG785D steel were mainly gas metal arc welding (GMAW) (Ref 1). But the welding speed was relatively low, which may cause wider heat-affected zone (HAZ) and coarse microstructures as well as deformation and residual stress. As a result, welding efficiency was low and could not meet the need. Therefore, new joining techniques for the steel were expected to be explored (Ref 2). If advanced joining techniques for the steel were successfully implemented, it could reduce the manufacturing time and the need for skilled labor, which led to a decrease in costs associated with the welding process and thus improved the joint quality.

Qiang Zhang, Jianmin Han, Zhiyong Yang, and Junqiang Wang, School of Mechanical, Electronic and Control Engineering, Beijing Jiaotong University, Beijing 100044, China; and **Caiwang Tan,** Shandong Provincial Key Laboratory of Special Welding Technology, Harbin Institute of Technology, Weihai 264209, China. Contact e-mails: jmhan@bjtu.edu.cn and tancaiwang@163.com.

Electron beam welding (EBW) process, as a mature advanced manufacturing technology, has demonstrated the great potential for thick plate welding in a single pass due to its higher power density at a shorter interaction time (Ref 3-7). The welded specimen is characterized by a higher depth-to-width ratio, narrower fusion zone and HAZ. The chance of grain coarsening was expected to reduce and thereafter distortion of thick plate because of considerably lower heat input compared to conventional arc welding processes (Ref 8, 9). In addition, the use of EBW process in a vacuum environment could prevent contamination of the molten pool from oxidation and other defects caused by involvement of atmospheric elements. Wiednig et al. (Ref 10) used EBW process to successfully realize 50-mm-thick-walled components made from nickel base alloy 625 and cast martensite 9% chromium steel without pre- and post-heating. The joints with good mechanical properties were obtained, and all quality requirements were fulfilled. Liu et al. (Ref 11) studied the effects of heterogeneity in the EBWed Ti6Al4 V alloy and found that the heterogeneous microstructures formed at the weld decreased the mechanical properties compared to uniform microstructure of base metal. Lakshminarayanan et al. (Ref 12) investigated the microstructures and mechanical properties of EBWed 4-mm-thick AISI ferritic stainless steel joints. The coarse ferrite grains in the base metal were found to transform into fine equiaxed axial grains and columnar grains because of rapid solidification. In addition, the results obtained from EBW of thick plated Inconel 718 and titanium alloys also confirmed the feasibility that acceptable joints without obvious defects and good quality were achieved (Ref 13, 14). The microstructures and mechanical properties in weld metal and HAZ were usually comparatively investigated since the great differences of microstructures and mechanical properties existed between the two zones caused by thermal cycle (Ref 15).

In our previous study (Ref 1), the GMAW of HG785D steel was studied. The microstructures and mechanical properties

Table 1 Chemical compositions and mechanical properties of HG785D steel

Elements									Mechanical properties		
C	Si	Mn	Ni	Cr	Mo	Nb	P	S	Tensile strength	Elongation	Impact energy (−20 °C)
0.12	0.40	1.8	0.75	0.70	0.50	0.06	0.025	0.015	880 MPa	15%	92 J

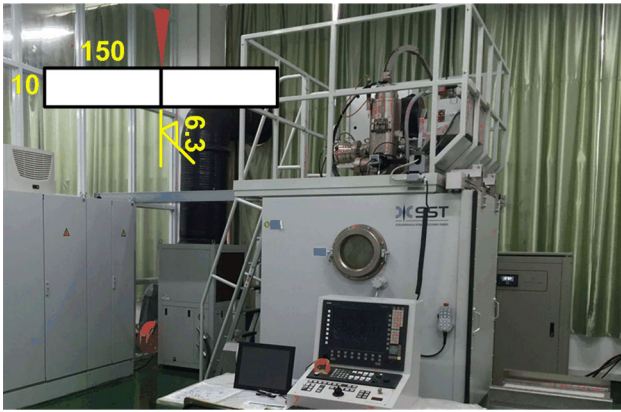


Fig. 1 Experimental setup of electron beam welding process

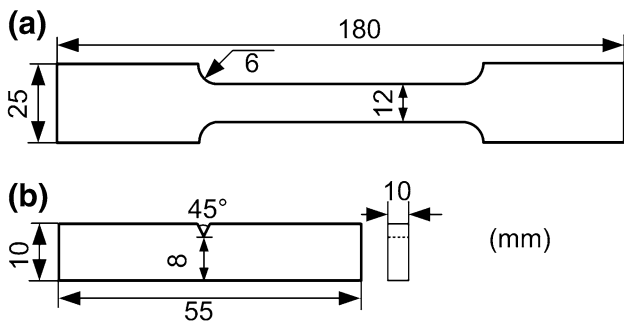


Fig. 2 Dimensions of the specimens used for tensile and impact tests: (a) tensile test and (b) impact test

between HAZ and weld metal were analyzed. HAZ had lower impact toughness and higher hardness compared to weld metal. To the best of our knowledge, electron beam welding of HG785D steel has not been investigated before. Therefore, in this work, EBW characteristics of HG785D steel were examined and its feasibility was investigated. After preliminary trials, microstructures and mechanical properties between HAZ and weld metal were comparatively characterized. In addition, the difference between electron beam welding and conventional arc welding was discussed.

2. Experimental

The materials used in the study were HG785D high-strength steels with dimensions of 350 mm × 150 mm × 10 mm. The nominal tensile strength was 785 MPa. The base metal was in quenched and tempered state. The chemical compositions are listed in Table 1. The plates were degreased by acetone and polished by abrasive paper before electron beam welding.

Figure 1 shows the experimental setup of electron beam welding process. The edges of the plates were carefully machined to obtain a square butt joint. The welding process was performed by EBW machine with 60-kV capacity. The vacuum degree in the experiments was 3×10^{-2} Pa. Full penetration in single pass was achieved by preliminary trials to optimize the welding parameters. After that, the beam current was varied during the welding process while other parameters were kept constant. The welding parameters used in the study were: accelerating voltage of 60 kV, focus current of 585 mA, welding speed of 650 mm/min. Electron beam current was varied from 75 mA to 90 mA by increment of 5 mA.

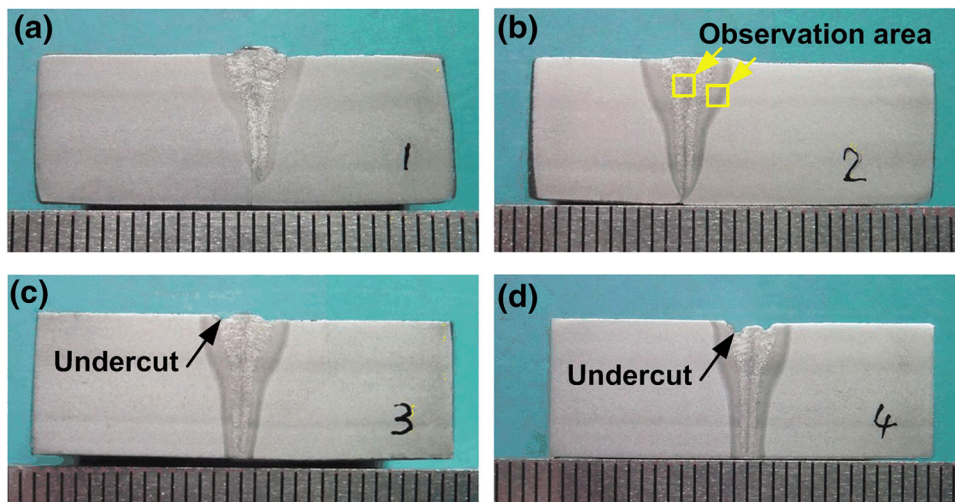


Fig. 3 Cross sections of electron beam-welded HG785D joints produced with different beam currents: (a) 75 mA, (b) 80 mA, (c) 85 mA and (d) 90 mA

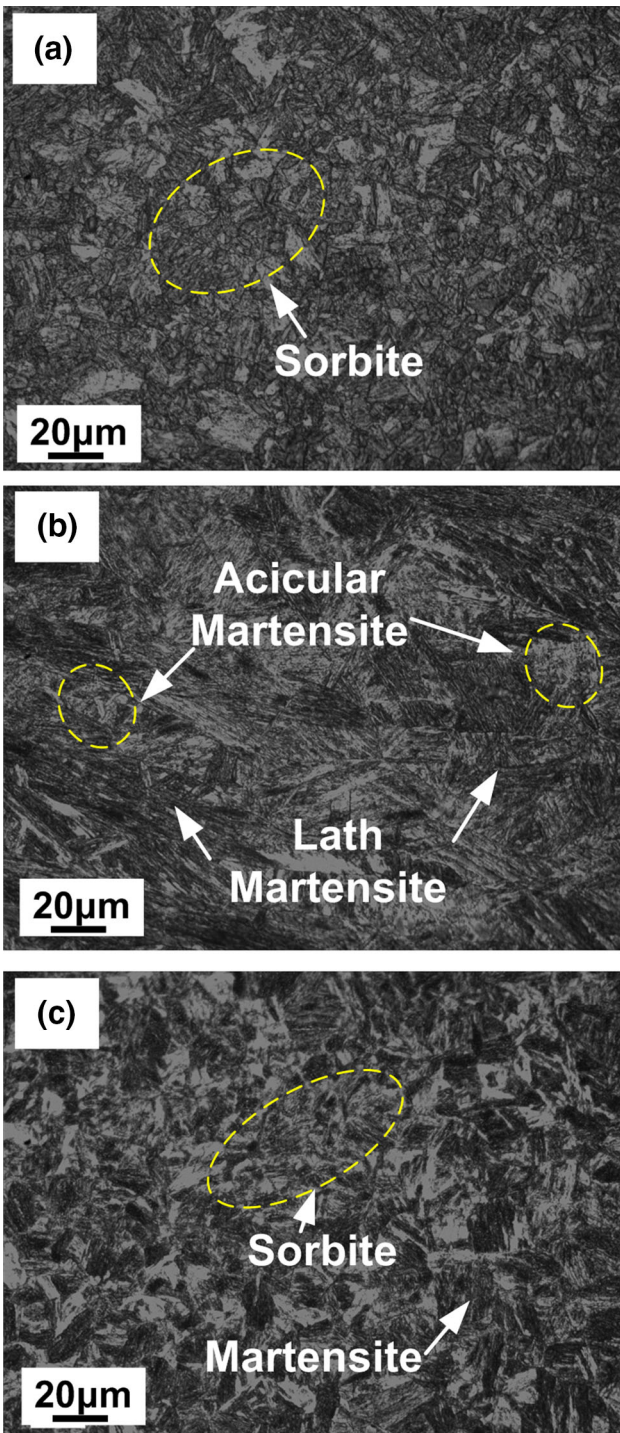


Fig. 4 Optical microstructure morphologies of HG785D steel electron beam-welded joints: (a) base metal, (b) weld metal and (c) HAZ

After the EBW process, typical cross sections of the welded specimens were cut. Standard grinding and polishing preparation procedures were then utilized. The appearances and cross sections were observed using an optical microscope (OM). For electron backscattered diffraction (EBSD) analysis, the polished samples for optical observation were then electropolished with a mixed solution of HClO_4 and $\text{C}_2\text{H}_5\text{OH}$ (1:9) at a voltage of 10 kV and dwell time 20 S. A thin foil was cut from

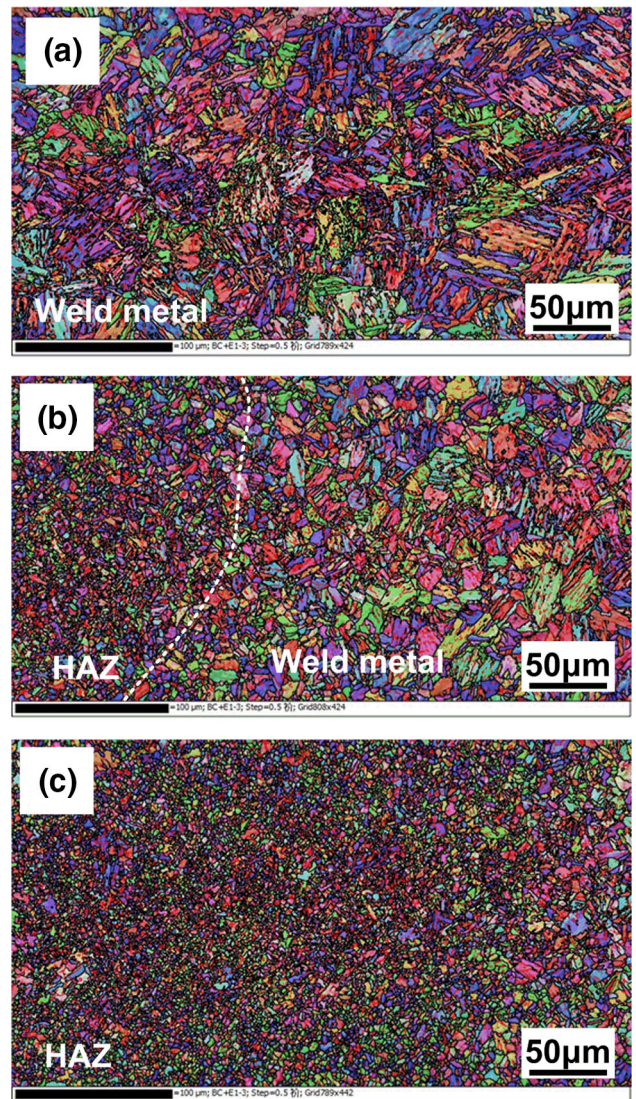


Fig. 5 EBSD micrographs showing the crystal orientation in the HG785D steel joints: (a) base metal, (b) weld metal and (c) HAZ

specimen and grinded to about 40 μm in thickness, followed by twin-jet electropolishing to obtain transmission electron microscopy (TEM) sample. TEM analysis was performed with a Tecnai G^2 F30 which was operated at a nominal voltage of 300 kV. Vickers hardness measurement was performed across the EBW joints. A test load of 10 Kgf and a dwell time of 30 s were utilized. Figure 2 shows the dimensions of the specimens used for tensile and impact tests. The tensile tests were performed at room temperature using Instron 5569 at a crosshead speed of 1 mm/min. Joint strength was calculated via the tensile testing of at least three specimens. The impact toughness of the weld metal and HAZ was evaluated by Charpy impact test. To evaluate the impact toughness of the weld metal and HAZ, the notch was machined at the weld metal as well as in the HAZ, respectively. Impact testing was performed at $-20\text{ }^\circ\text{C}$ using a pendulum-type impact testing machine. The amount of energy absorbed in fracture was recorded, and the absorbed energy was defined as the impact toughness of the material.

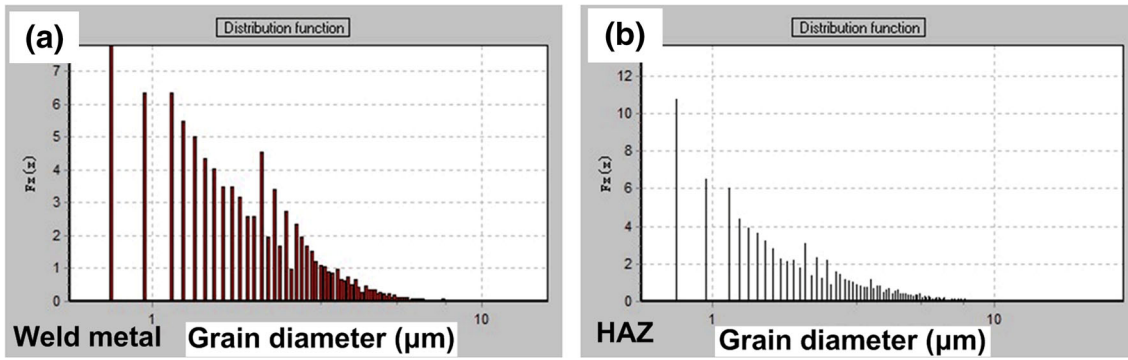


Fig. 6 Histogram of grain size distribution: (a) weld metal and (b) HAZ

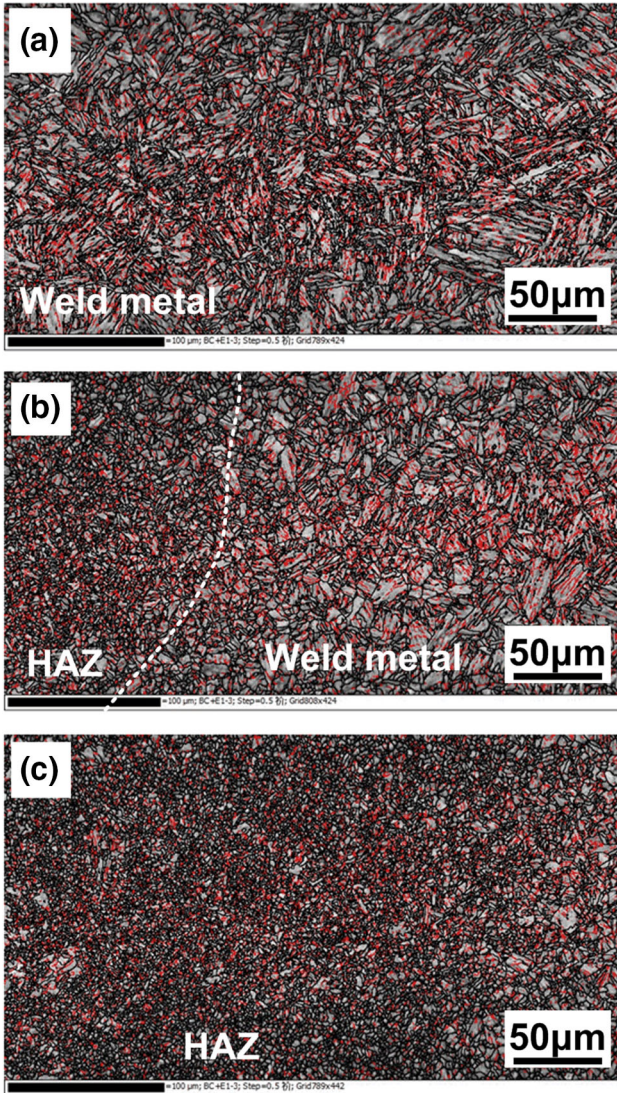


Fig. 7 Grain boundary characterization distribution maps: (a) weld metal, (b) line between HAZ and weld metal, and (c) HAZ

3. Results

3.1 Weld Appearance

Figure 3 shows typical appearances of HG785D steel EBWed joints made with different beam currents. Small and

incomplete penetration was observed when using small beam current, as shown in Fig. 3(a). With the increase in beam current, the penetration increased. Visually acceptable without obvious defects were achieved when the beam current was 80 mA. The weld with high depth-to-width ratio was successfully achieved in this case. Excessive penetration was observed with further increase in current. However, undercut was produced with the increasing beam current of more than 85 mA as shown in Fig. 3(c) and (d). The defect would be detrimental to the mechanical properties and should be avoided in the optimized joints. Therefore, the joint produced at the optimized beam current of 80 mA was analyzed in the following part based on the appearance.

3.2 Microstructures

Figure 4 shows optical micrographs taken at different regions of the EBWed joint welded at the beam current of 80 mA. As shown in Fig. 4(a), the as-received base metal mainly consisted of fine tempered sorbite. After the EBW process, weld metal microstructure was found to exhibit coarse lath martensite with small amount of acicular martensite indicated in Fig. 4(b). The HAZ microstructure was, however, evolved to martensite mingled with some tempered sorbite. From these observations, it could be inferred that the grain size grew up moving from base metal to weld metal when the microstructure changed from fine tempered sorbite to coarse lath martensite. In order to reveal the feature of crystal orientation, EBSD mapping was performed and the results are shown in Fig. 5. In the figure, different color indicated grain misorientation was greater than 15° and single color region represents the crystals with the same orientation. It was clearly visible that the grain size in the weld metal was far larger than that in the HAZ as shown in Fig. 5(b). According to Hall–Petch equation, yield stress σ_y is related to grain size d , $\sigma_y = \sigma_0 + k_y d^{1/2}$, where σ_0 is friction stress and k_y is a material-dependent constant known as the H-P slope that measures the relative strengthening contribution of grain boundaries, and d is the average grain size (Ref 16). Therefore, the strength in the HAZ was expected to be higher than that in the weld metal.

Figure 6 shows histogram of grain size distribution corresponding to weld metal and HAZ. The average effective grain size in these two regions was $5.623 \mu\text{m}$ and $3.217 \mu\text{m}$, respectively. It suggested the average effective grain size in the weld metal was much larger than that in the HAZ. In addition, it could be found from histogram that the proportion of large grain size was higher in the weld zone than that in the

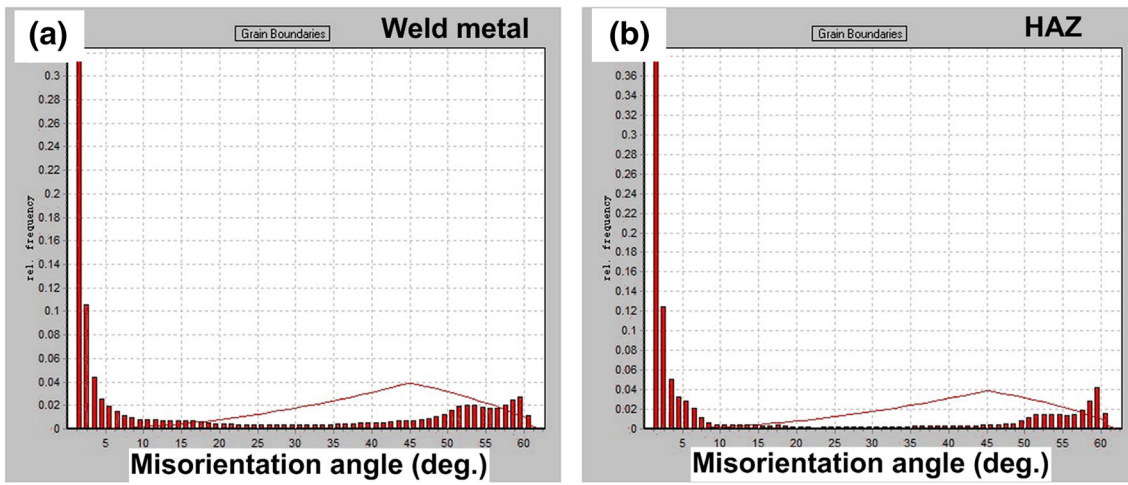


Fig. 8 Misorientation angle distribution of grain boundary: (a) weld metal and (b) HAZ

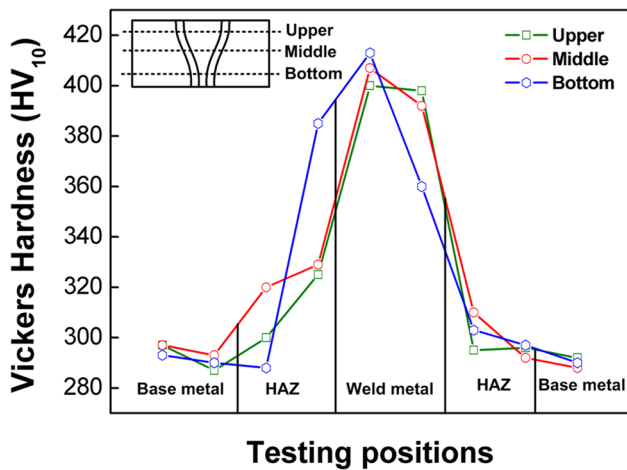


Fig. 9 Hardness profile distribution of electron beam-welded HG785D steel joint

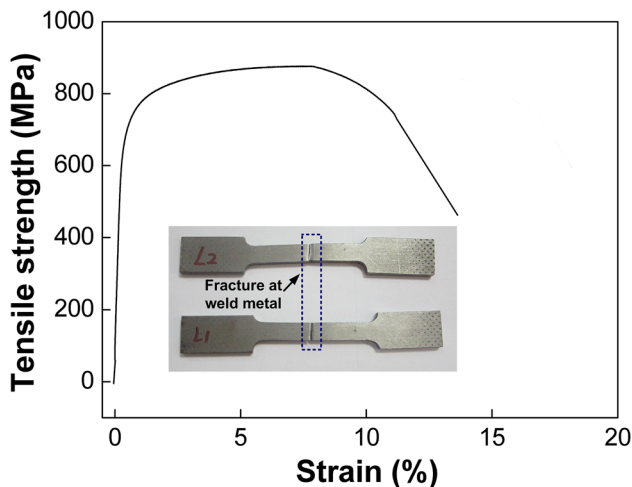


Fig. 10 Tensile testing curve and fracture location on joint welded at beam current of 80 mA

HAZ. It was attributed to the nucleation and transformation of martensite in the weld metal. The microstructure transformation was inhibited in the HAZ due to low heat input.

Figures 7 and 8 show grain boundary characterization distribution maps and grain orientation distribution of the misorientation angles. Red line indicated the locations of low-angle grain boundaries (LAGBs) with misorientation between 2° and 15° , and black line indicated the locations of high-angle grain boundaries (HAGBs) with misorientation greater than 15° . The volume fraction of LAGBs accounted for 38% via the statistics distribution of grain orientation in the weld metal, while 30% in the HAZ. Small angle boundaries with refining tempered sorbite existed in the HAZ, making it contain high density dislocation and tiny substructure. The presence of these in the HAZ effectively prevented crack propagation, leading to high mechanical properties.

3.3 Mechanical Properties

3.3.1 Hardness Distribution. Figure 9 shows Vickers hardness profile distribution across HG785D steel EBWed joint. The schematic of measurement points is shown in the inset of Fig. 9. The hardness of the as-received base metal was approximately 297 HV. The average hardness at the HAZ increased to the range of 300–325 HV since some base metals were transformed to martensite. The hardness at weld metal was the highest among three regions, with maximum value of 400 HV. This variation was closely associated with the microstructure transformation shown in Fig. 4. The slight difference of hardness value among the top, middle and bottom of the welds was observed, which was related to the different thermal gradient in thickness. Therefore, cooling rate was varied giving rise to the different microstructure distribution.

3.3.2 Tensile Strength. Figure 10 shows the fracture location of EBWed joints with the optimized parameter of beam current of 80 mA. The average tensile strength reached 869 MPa (elongation rate of 12%), which was 98.8% of that of base metal. All the joints fractured at the weld, indicating it was the weak region at the joint. This was closely associated with the microstructure evolution as discussed in section 3.2. Fracture surface of the tensile specimens obtained at different beam currents was observed and the results are shown in Fig. 11. The fracture surface of joint welded at beam current 80 mA was characterized by uniform and ductile dimples as shown in Fig. 11(a) and (b). It indicated the joint failure was ductile fracture. In comparison, when the beam current was

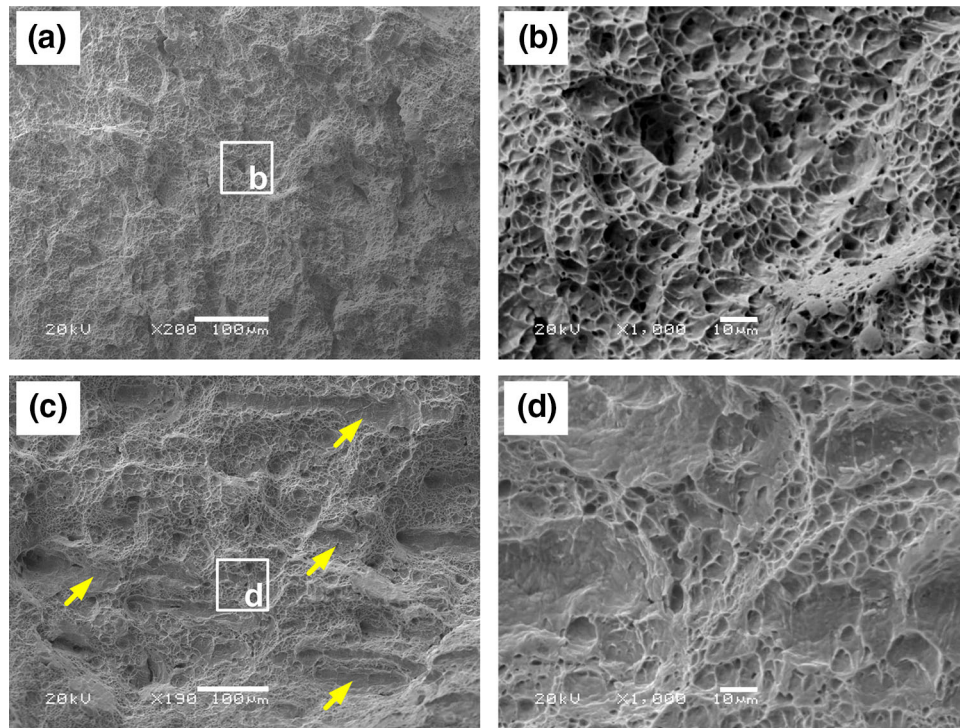


Fig. 11 Fracture surfaces of tensile testing on joints welded at different beam currents: (a) 80 mA, (b) magnified view of rectangle in (a), (c) 85 mA and (d) magnified view of rectangle in (c)

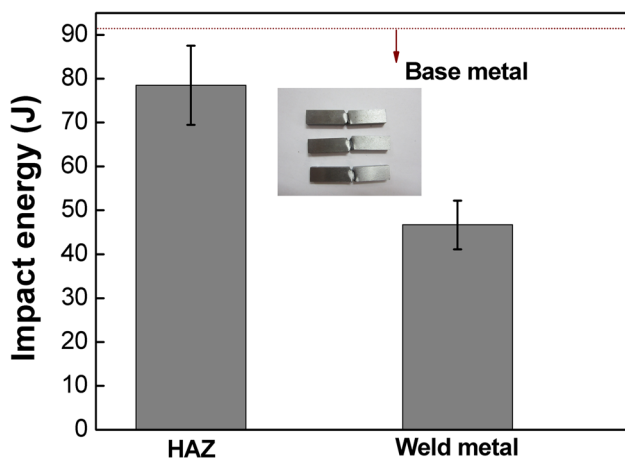


Fig. 12 Impact toughness of HAZ and weld metal

85 mA, partially cleavage fracture which is arrowed in Fig. 11(c) and magnified in Fig. 11(d) was observed at the fracture surface of the joint besides some shallow dimples. It suggested the presence of undercut defect produced with higher beam current could cause a sharp decrease in joint strength and brittle fracture behavior.

3.3.3 Impact Toughness. Charpy impact toughness of the EBWed joint was evaluated, and the result is shown in Fig. 12. The average impact toughness of HAZ and weld metal at $-20\text{ }^{\circ}\text{C}$ were 78 and 46 J, respectively. It was clear that the HAZ exhibited higher impact toughness than the weld metal. Figure 13 displays the fracture surfaces of impact tested specimens at the HAZ and the weld metal, respectively. The fracture surface of weld metal exhibited flat and cleavage characteristics. However, the fine dimples were observed from the fracture surfaces of HAZ.

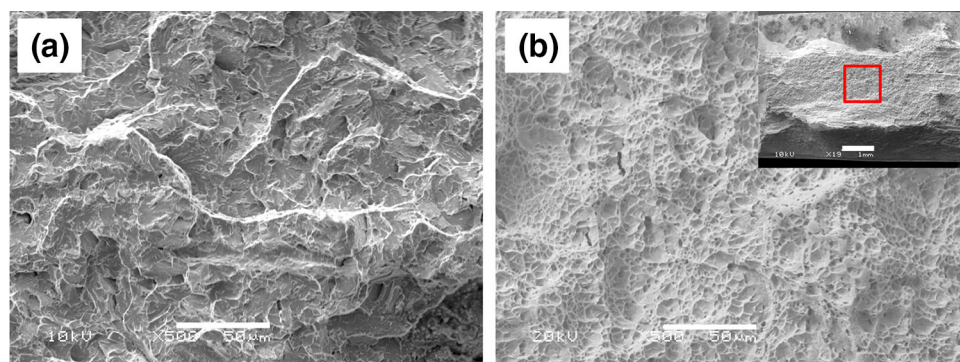


Fig. 13 Fracture surfaces of impact toughness: (a) weld metal and (b) HAZ

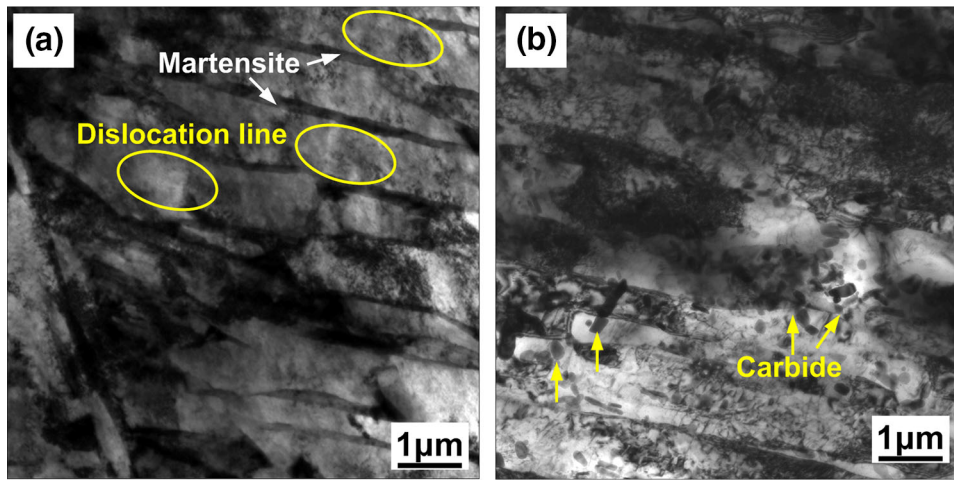


Fig. 14 TEM images taken at different areas: (a) weld metal and (b) HAZ

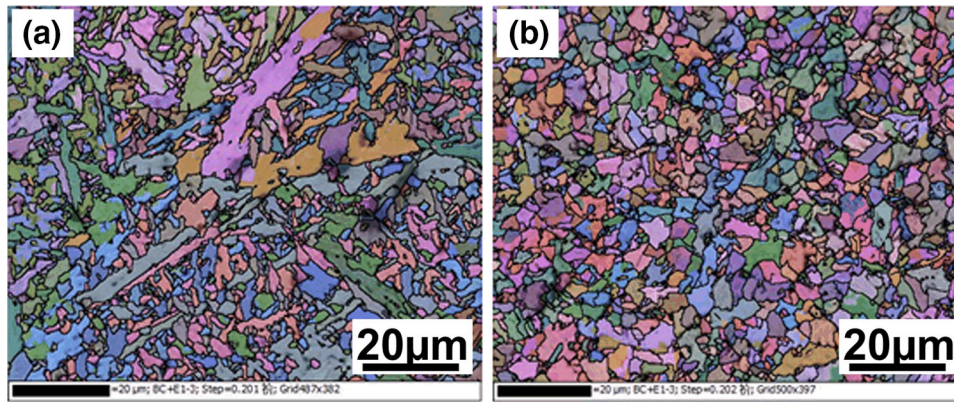


Fig. 15 EBSD micrographs of MAG-welded joint: (a) HAZ, (b) weld metal

4. Discussion

Based on the aforementioned results, it is feasible for EBW process to weld thick plated HG785D steel in appropriate welding parameters and the joint exhibited good mechanical properties. No solidification cracking was observed at the weld metal or HAZ, which was usually evidenced when using arc welding (Ref 17, 18). Microstructure studies also indicated the absence of grain coarsening effects at the HAZ.

Electron beam welding is known for its higher cooling rates, higher depth-to-width ratio. During the electron beam welding process, the weld metal was heated to a high temperature resulting in the rapid growth of austenite since base metal was in quenched and tempered state. Upon fast cooling, the microstructure in the weld seam was rapidly transformed into the coarse martensite. While HAZ did not grow at the same time with the action of low heat input, small part of it was transformed into the martensite while large part still remained the tempered sorbite. As a result, the mixed structure of martensite and refined tempered sorbite existed in the HAZ. That was the main reason for the formation of different microstructure in weld metal and HAZ and thereafter the mechanical properties.

To further confirm the difference between the HAZ and the weld metal, TEM analysis concerning microstructure at two different zones were performed and the results are shown in

Fig. 14. Lath-like characteristics of martensite was clearly observed from the TEM image, where dense and mingled dislocation lines were found in the martensite crystal as arrowed in the figure. The ductility and toughness of martensite was dependent on the submicrostructure which hindered the nucleation and propagation of cracks (Ref 19), while in the HAZ, granular carbide was observed in the ferrite matrix as shown in Fig. 14(b), which was typical morphology of tempered sorbite. The incomplete transformation was confirmed, and the presence of sorbite improved the toughness of the HAZ. Therefore, embrittlement of HAZ was avoided. Good mechanical properties shown in Fig. 10 and 12 were thus achieved. With the combined effect, the tensile strength and impact toughness of HAZ was higher than that of weld metal. It suggested the inhomogeneous microstructure along the welded joint had a direct relationship with the mechanical properties. The microstructure, hardness and strength in HAZ and weld were also investigated by Zhu et al. (Ref 20-22). Good agreement was established for the correlated strength and experimental observation of microstructure.

The aforementioned results were significantly different from the obtained results when using GMAW process. Figure 15 shows the EBSD mapping taken at the GMAWed HG785D steel joint. The case was just the opposite of that in the EBW process. The microstructure at the weld metal was uniform and dense. While the microstructure at HAZ was heated and changed into coarse martensite due to larger heat input

compared to the EBW process. Therefore, the hardness at the HAZ was higher than that of weld metal. Impact toughness of weld metal was found to be better than that of HAZ.

5. Conclusions

The microstructure and mechanical properties between weld metal and HAZ in EBWed HG785D steel joints were comparatively investigated. From this investigation, the following conclusions could be drawn:

1. Electron beam welding of 10-mm-thick HG785D steel was successfully achieved. Visually acceptable joints without obvious defects were obtained by adjusting beam current. The strength of joint welded at optimized parameters could reach 869 MPa, which was 98.8% of that of base metal.
2. The microstructure at the weld metal consisted of coarse lath martensite and a small amount of acicular martensite, while that in the HAZ was tempered sorbite and martensite. The grain size in the weld was found to be larger than that in the HAZ, and the proportion of large grain size in the weld zone was higher than that in the HAZ.
3. The hardness in the weld metal was higher than the HAZ and base metal. The tensile strength and impact toughness in the HAZ was higher than that in the weld metal. The fracture surfaces of tensile test and impact test on the optimized joint were characterized by uniform and ductile dimples, while flat and cleavage or shallow dimples were observed at the non-optimized joint.

Acknowledgments

The research was financially supported by Postdoctoral Science Foundation of China (No. 2015M571406).

References

1. Q. Zhang, J. Han, Z. Yang, and J. Wang, Properties of Heat Affected Zone for HG785D High Strength Steel, *Trans. China Weld. I.*, 2014, **35**, p 109–112 (**In Chinese**)
2. R. Zhong, F. Chen, C. Liu, and P. Zhang, Microstructure and Properties of Laser Welding and CO₂ Welding of HG785 High Strength Structure Steel, *Appl. Laser*, 2011, **31**(2), p 147–150 (**In Chinese**)
3. B. Zhang, X. Li, T. Wang, and X. Wang, Microstructure and Corrosion Behavior of Zr-702 Joined by Electron Beam Welding, *Vacuum*, 2015, **121**, p 159–165
4. B.G. Zhang, J. Zhao, X.P. Li, and J.C. Feng, Electron Beam Welding of 304 Stainless Steel to QCr0.8 Copper Alloy with Copper Filler Wire, *Trans. Nonferr Metal Soc.*, 2014, **24**, p 4059–4066
5. S.Q. Wang, W.Y. Li, Y. Zhou, X. Li, and D.L. Chen, Tensile and Fatigue Behavior of Electron Beam Welded Dissimilar Joints of Ti–6Al–4 V and IM1834 Titanium Alloys, *Mater. Sci. Eng., A*, 2016, **649**, p 146–152
6. X. Zhan, J. Chen, J. Liu, Y. Wei, J. Zhou, and Y. Meng, Microstructure and Magnesium Burning Loss Behavior of AA6061 Electron Beam Welding Joints, *Mater. Des.*, 2016, doi:10.1016/j.matdes.2016.03.058
7. S. Wang and X. Wu, Investigation on the Microstructure and Mechanical Properties of Ti–6Al–4 V Alloy Joints with Electron Beam Welding, *Mater. Des.*, 2012, **36**, p 663–670
8. Y. Qi, J. Deng, Q. Hong, and L. Zeng, Electron Beam Welding, Laser Beam Welding and Gas Tungsten Arc Welding of Titanium Sheet, *Mater. Sci. Eng., A*, 2000, **280**, p 177–181
9. T. Pasang, J.M.S. Amaya, Y. Tao, M.R. Amaya-Vazquez, F.J. Botana, J.C. Sabol et al., Comparison of Ti–5Al–5 V–5Mo–3Cr Welds Performed by Laser Beam, Electron Beam and Gas Tungsten Arc Welding, *Procedia Eng.*, 2013, **63**, p 397–404
10. C. Wiednig, C. Lochbichler, N. Enzinger, C. Beal, and C. Sommitsch, Dissimilar Electron Beam Welding of Nickel Base Alloy 625 and 9% Cr Steel, *Procedia Eng.*, 2014, **86**, p 184–194
11. J. Liu, X.L. Gao, L.J. Zhang, and J.X. Zhang, Effects of the Heterogeneity in the Electron Beam Welded Joint on Mechanical Properties of Ti6Al4 V Alloy, *J. Mater. Eng. Perform.*, 2015, **24**, p 315–328
12. A.K. Lakshminarayanan, V. Balasubramanian, and G. Madhusudhan Reddy, Microstructure and Mechanical Properties of Electron Beam-Welded AISI, 409 M-Grade Ferritic Stainless Steel, *Int. J. Adv. Manuf. Technol.*, 2010, **55**, p 153–162
13. G. Madhusudhana Reddy, C.V. Srinivasa Murthy, K. Srinivasa Rao, and K. Prasad Rao, Improvement of Mechanical Properties of Inconel 718 Electron Beam Welds—Influence of Welding Techniques and Postweld Heat Treatment, *Int. J. Adv. Manuf. Technol.*, 2008, **43**, p 671–680
14. B. Wu, J. Li, and Z. Tang, Study on the Electron Beam Welding Process of ZTC4 Titanium Alloy, *Rare Metal Mat. Eng.*, 2014, **43**, p 786–790
15. Y. Mei, Y. Liu, C. Liu, C. Li, L. Yu, Q. Guo et al., Effect of Base Metal and Welding Speed on Fusion Zone Microstructure and HAZ Hot-Cracking of Electron-Beam Welded Inconel 718, *Mater. Des.*, 2016, **89**, p 964–977
16. D. Du, R. Fu, Y. Li, L. Jing, J. Wang, Y. Ren et al., Modification of the Hall-Petch Equation for Friction-Stir-Processing Microstructures of High-Nitrogen Steel, *Mater. Sci. Eng., A*, 2015, **640**, p 190–194
17. I. Brown, The Role of Microsegregation in Centreline Cold Cracking of High Strength Low Alloy Steel Weldments, *Scripta Mater.*, 2006, **54**, p 489–492
18. W. Xue, Q.G. Pan, Y.Y. Ren, W. Shang, H.Q. Zeng, and H. Liu, Microstructure and Type IV Cracking Behavior of HAZ in P92 Steel Weldment, *Mater. Sci. Eng., A*, 2012, **552**, p 493–501
19. C. Du, J.P.M. Hoefnagels, R. Vaes, and M.G.D. Geers, Block and Sub-block Boundary Strengthening in Lath Martensite, *Scripta Mater.*, 2016, **116**, p 117–121
20. M.L. Zhu and F.Z. Xuan, Effect of microstructure on strain hardening and strength distributions along a Cr–Ni–Mo–V steel welded joint, *Mater. Des.*, 2015, **65**, p 707–715
21. M.L. Zhu, D.Q. Wang, and F.Z. Xuan, Effect of Long-term Aging on Microstructure and Local Behavior in the Heat-Affected Zone of a Ni–Cr–Mo–V Steel Welded Joint, *Mater. Charact.*, 2014, **87**, p 45–61
22. M.L. Zhu and F.Z. Xuan, Correlation Between Microstructure, Hardness and Strength in HAZ of Dissimilar Welds of Rotor Steels, *Mater. Sci. Eng., A*, 2010, **527**, p 4035–4042